



Supplement of

Drivers of CO₂ emissions during the dry phase in Mediterranean and Temperate ponds

Victoria Frutos-Aragón et al.

Correspondence to: Victoria Frutos-Aragón (victoriavfa@gmail.com) and Sandra Brucet (sandra.brucet@uvic.cat)

The copyright of individual parts of the supplement might differ from the article licence.

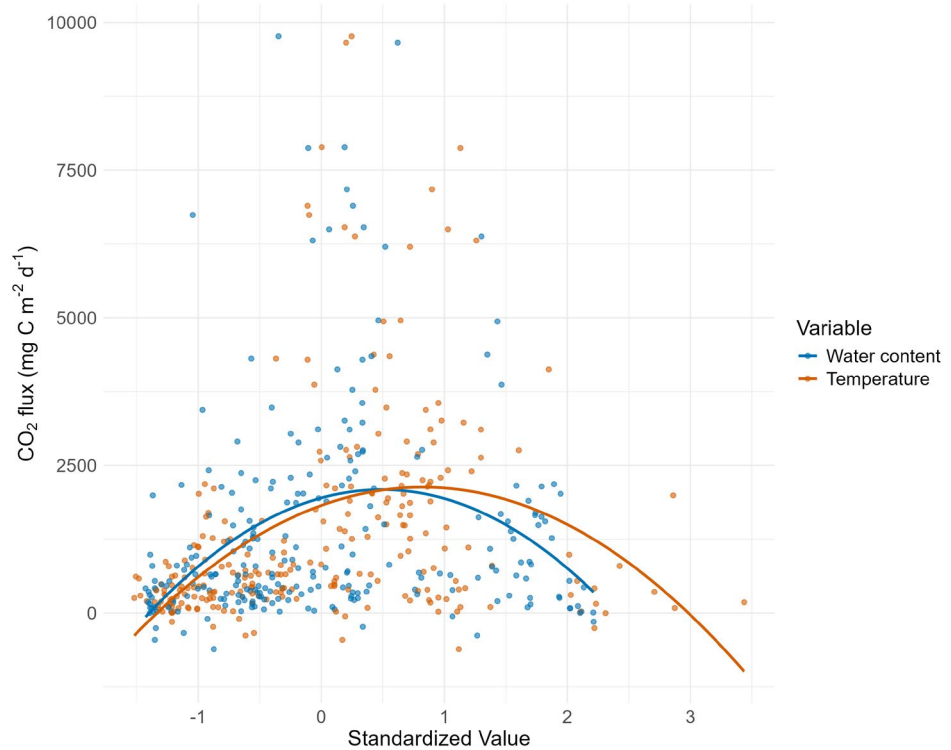
Table S1. Summary of CO₂ fluxes by season. For each pond, the table shows the mean \pm standard deviation (SD) of CO₂, the observed range (maximum to minimum) values and the number of samples (N).

CO ₂ fluxes (mg C m ⁻² d ⁻¹)								
Pond	Country	Climate	Summer			Autumn		
			(Mean \pm SD)	(Max to Min)	N	(Mean \pm SD)	(Max to Min)	N
SP008	Spain	Mediterranean	2216 \pm 878	3438 — 968	5	1079 \pm 956	1755 — 403	2
SP014	Spain	Mediterranean	2364 \pm 1145	3779 — 663	7	542 \pm 205	811 — 238	7
SP019	Spain	Mediterranean	1573 \pm 757	2903 — 376	9	469 \pm 506	1560 — 338	9
SP026	Spain	Mediterranean	190 \pm 383	538 — 454	6	346 \pm 190	603 — 98	6
SP028	Spain	Mediterranean	6289 \pm 2693	9765 — 2160	6	259 \pm 442	817 — 234	4
SP029	Spain	Mediterranean	3071 \pm 1919	6308 — 1501	5	741 \pm 304	1147 — 435	5
SP030	Spain	Mediterranean	5356 \pm 2111	7873 — 2692	6	198 \pm 108	338 — 62	6
SP032	Spain	Mediterranean	2503 \pm 973	4126 — 761	9	405 \pm 283	890 — 25	9
SP035	Spain	Mediterranean	2133 \pm 1088	3224 — 395	5	489 \pm 504	1211 — 40	4
SP040	Spain	Mediterranean	3815 \pm 3116	6200 — 289	3	-	-	0
SP041	Spain	Mediterranean	295 \pm 148	421 — 100	4	-	-	0
SP043	Spain	Mediterranean	684 \pm 899	1991 — 20	4	-	-	0
SP044	Spain	Mediterranean	46 \pm 221	359 — 256	5	558 \pm 291	991 — 228	6
SP045	Spain	Mediterranean	452 \pm 598	1109 — 611	6	-	-	0
SP046	Spain	Mediterranean	487 \pm 342	988 — 235	4	396 \pm 220	616 — 127	5
SP049	Spain	Mediterranean	242 \pm 280	798 — 24	6	243 \pm 179	471 — 62	5
BE059	Belgium	Temperate	-	-	0	1726 \pm 1762	4308 — 347	4
BE065	Belgium	Temperate	-	-	0	725 \pm 224	937 — 414	4
DE001	Germany	Temperate	-	-	0	491 \pm 248	785 — 147	6
DE007	Germany	Temperate	1079 \pm 680	2143 — 459	7	-	-	0
DE011	Germany	Temperate	4889 \pm 1085	6378 — 3866	4	-	-	0
DE012	Germany	Temperate	1391 \pm 305	1677 — 857	6	-	-	0
DE016	Germany	Temperate	-	-	0	452 \pm 468	718 — 381	5
DE019	Germany	Temperate	2333 \pm 576	2814 — 1424	5	1534 \pm 490	2108 — 1113	5
DE028	Germany	Temperate	1669 \pm 634	2291 — 696	6	365 \pm 530	1252 — 99	5
DE030	Germany	Temperate	1831 \pm 309	2156 — 1490	4	136 \pm 104	277 — 26	6
DE031	Germany	Temperate	-	-	0	1666 \pm 332	2182 — 1268	5
DK018	Denmark	Temperate	3656 \pm 3755	9657 — 55	6	353 \pm 51	389 — 317	2
DK034	Denmark	Temperate	-	-	0	440 \pm 281	868 — 201	5
DK042	Denmark	Temperate	-	-	0	127 \pm 269	634 — 148	6

Table S2. Comparison of environmental variables between climate regions. Results of Mann–Whitney U tests comparing the distributions of values between Mediterranean and Temperate ponds. Statistically significant differences ($p < 0.05$) are highlighted in bold.

Variable	Mediterranean		Temperate		p-value
	Mean	SD	Mean	SD	
Temperature 40 (K)	287.31	1.57	282.44	0.47	< 0.001
Precipitation 40 (mm S⁻¹)	2.52	0.64	1.97	0.19	< 0.01
Annual temperature (°C)	15.97	1.70	10.80	0.54	< 0.001
<i>Annual precipitation (mm)</i>	0.08	0.02	0.07	0.01	n.s.
<i>Hydroperiod length (months)</i>	6.29	3.52	9.15	2.31	n.s.
<i>Area (m²)</i>	2884.14	4827.94	912.00	773.62	n.s.
<i>Max depth (Cm)</i>	111.82	27.73	104.08	54.53	n.s.
Coverage (%)	59.75	22.12	84.29	31.59	< 0.01
<i>PVI (%)</i>	55.36	36.41	37.65	35.64	n.s.
<i>Conservation status</i>	72.68	17.17	79.79	16.23	n.s.
Sediment temperature (° C)	20.44	8.52	15.91	5.26	< 0.01
Water content (%)	22.97	13.47	55.42	24.40	< 0.001
<i>pH</i>	6.54	1.08	6.70	0.72	n.s.
<i>Conductivity (µS cm⁻¹)</i>	420.26	269.29	603.52	500.30	n.s.
<i>Carbonate content (%)</i>	4.76	7.54	4.31	5.72	n.s.
Organic matter (%)	10.21	9.57	23.07	18.93	< 0.05
DOC (mg C g⁻¹)	1.02	1.71	2.77	3.67	< 0.05
Absorbance 254	0.24	0.23	0.57	0.44	< 0.01
<i>Absorbance 300</i>	16.79	8.11	20.23	8.78	n.s.
SUVA (L mg C⁻¹ m⁻¹)	1.89	0.87	1.35	1.54	< 0.05
<i>BIX</i>	0.53	0.07	0.58	0.18	n.s.
<i>FI</i>	1.21	0.11	1.21	0.13	n.s.
<i>HIX</i>	0.87	0.06	0.84	0.11	n.s.
<i>C1</i>	42.66	8.61	41.81	9.72	n.s.
C2	42.70	6.88	37.70	5.97	< 0.01
<i>C3</i>	14.64	7.47	20.50	12.89	n.s.
<i>Open nature 100 (%)</i>	29.67	36.35	8.85	16.21	n.s.
<i>Forest 100 (%)</i>	34.38	33.94	18.59	18.13	n.s.
Pasture 100 (%)	3.61	10.59	29.86	27.47	< 0.001
<i>Arable 100 (%)</i>	31.99	41.57	31.24	29.24	n.s.
<i>Grassland 100 (%)</i>	0.00	0.00	3.78	12.55	n.s.
Urban 100 (%)	0.35	1.28	7.69	15.78	< 0.05
<i>Open nature 5 (%)</i>	50.81	29.17	29.73	39.28	n.s.
<i>Forest 5 (%)</i>	41.91	31.61	28.97	34.10	n.s.
Pasture 5 (%)	3.80	13.29	25.96	35.59	< 0.01
<i>Arable 5 (%)</i>	3.48	12.77	14.33	31.24	n.s.
<i>Grassland 5 (%)</i>	0.00	0.00	1.03	2.88	n.s.
<i>Urban 5 (%)</i>	0.00	0.00	0.00	0.00	n.s.
TN water (mg L⁻¹)	1.91	1.24	4.29	4.88	< 0.05
TP water (mg L⁻¹)	0.20	0.27	0.63	0.56	< 0.01
<i>DOC water (mg L⁻¹)</i>	26.49	18.83	21.64	9.95	n.s.
Chlorophyll a (µg L⁻¹)	20.53	21.65	54.73	47.67	< 0.05

Figure S1. Relationship between sediment water content, temperature and CO₂ fluxes. The plot shows the standardized relationship between sediment temperature and water content with CO₂ fluxes during the dry phase. Each point represents an individual observation, colour-coded by variable (orange = sediment temperature and blue = water content). Fitted quadratic regression lines depict the non-linear trends in the data.



Analysis of the dissolved organic matter components

We analysed the composition of organic matter components to assess their distribution across climate regions, seasons and hydroperiods, as well as their relationship with CO₂ fluxes. Significant differences were observed between climate regions in the humic-like component (C2) (Fig. S3a). In contrast, the overall composition of organic matter remained consistent across seasons (Fig. S2 and S3b). Regarding hydroperiod, we found a correlation between hydroperiod length and tryptophan-like component (C3) (Fig. S4). Moreover, the effect of these components on CO₂ fluxes was significant only during the summer, particularly for the humic-like (C2) and tryptophan-like (C3) components (Fig. S5).

Figure S2. PARAFAC-extracted components of dissolved organic matter by season (summer and autumn). C1 represents terrestrial humic-like substances (yellow), C2 humic-like (blue), and C3 tryptophan-like substances (green).

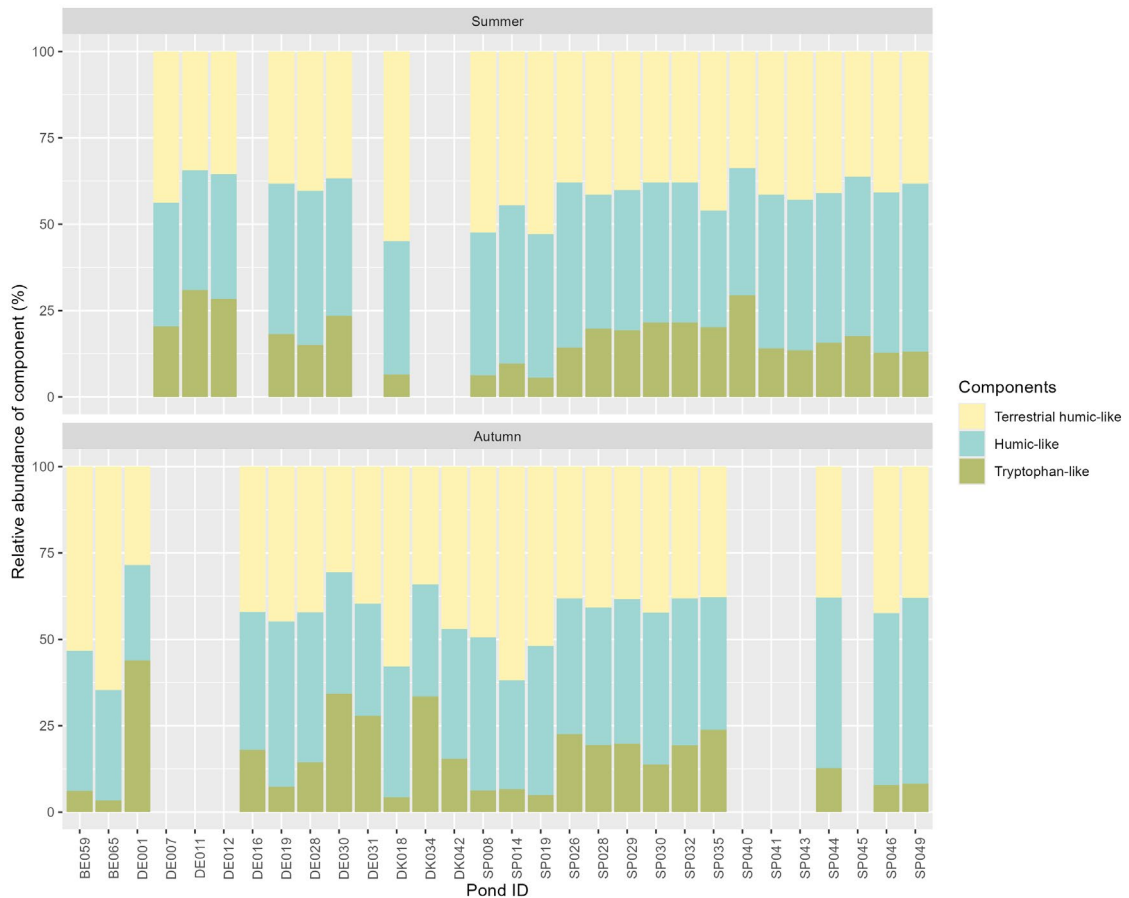


Figure S3. ANOVA results for dissolved organic matter components by climate regions (a) and seasons (b). C1 = terrestrial humic-like (yellow), C2 = humic-like (blue), and C3 = tryptophan-like (green). Asterisks (**) indicate significant differences between groups, $p < 0.01$; n.s. denotes non-significant differences.

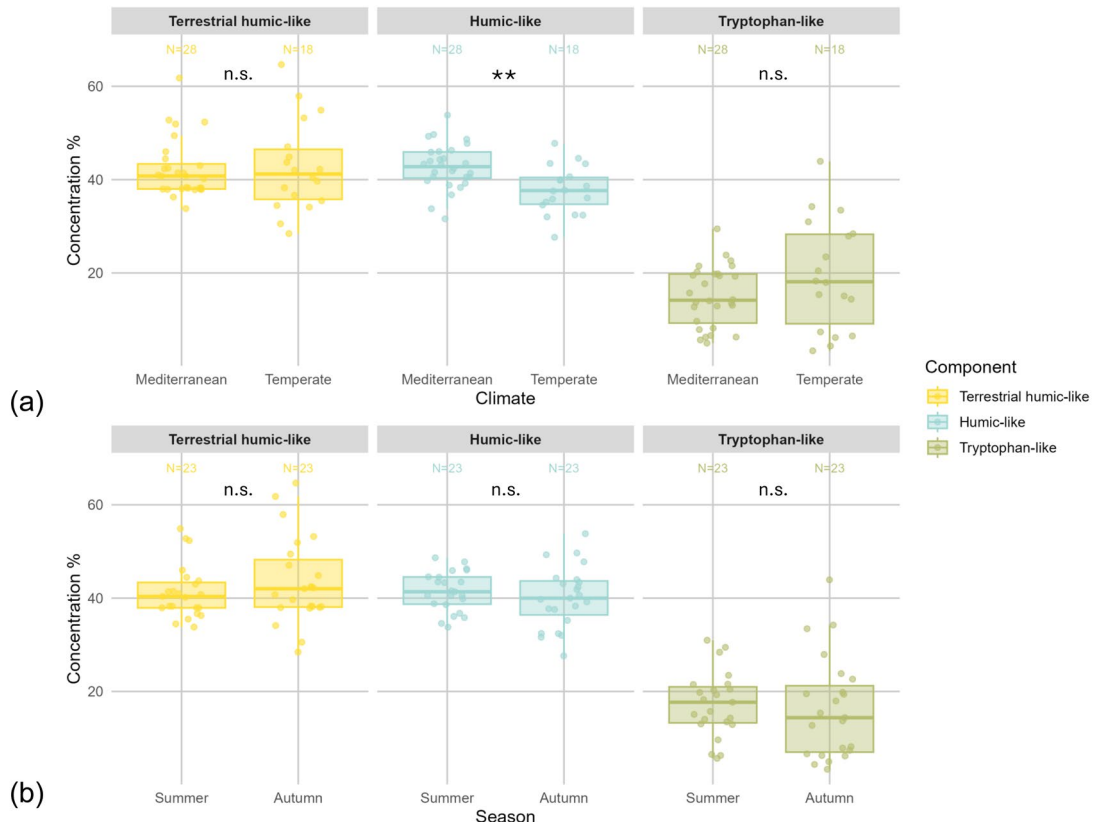


Figure S4. Scatterplots with fitted linear regressions (dashed lines) and 95% confidence intervals (grey shaded areas) showing the relationship between hydroperiod length and the concentration of three DOM components: C1 = terrestrial humic-like (yellow), C2 = humic-like (blue) and C3 = tryptophan-like (green). Each dot represents an individual pond measurement.

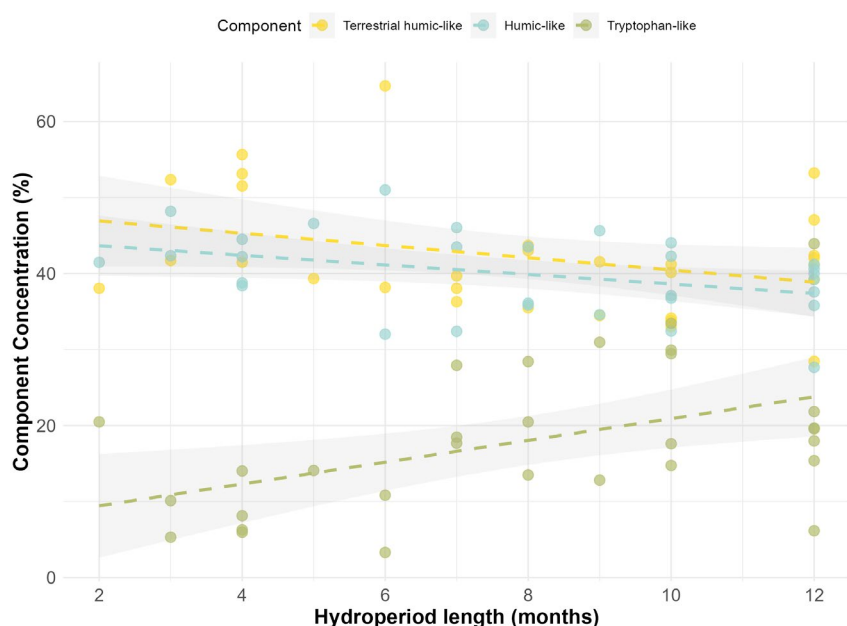


Figure S5. Relationship between CO₂ fluxes and the relative concentration (%) of fluorescent DOM components, grouped as terrestrial humic-like, humic-like, and tryptophan-like compounds. Each point represents the average CO₂ flux from a pond during the dry phase (summer or autumn). Lines show linear regressions with 95% confidence intervals (shaded areas), with blue indicating summer data and orange indicating autumn. Asterisks above each panel denote the significance of the interaction between component concentration and season on linear models: *** $p < 0.001$; * $p < 0.05$, n.s. denotes non-significant differences.

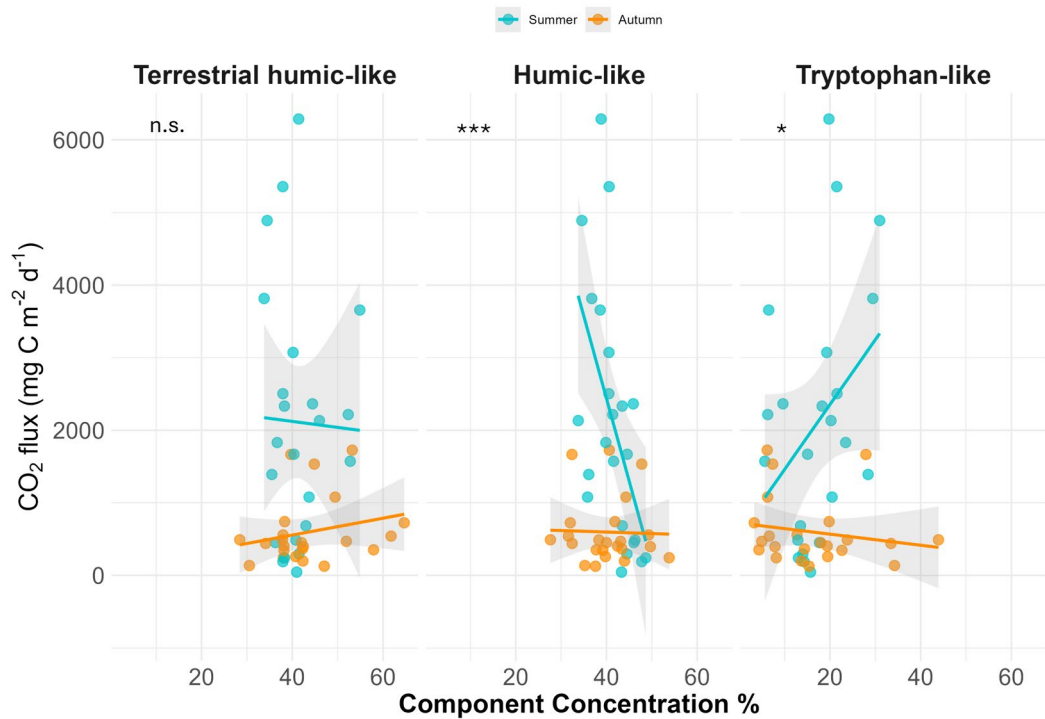
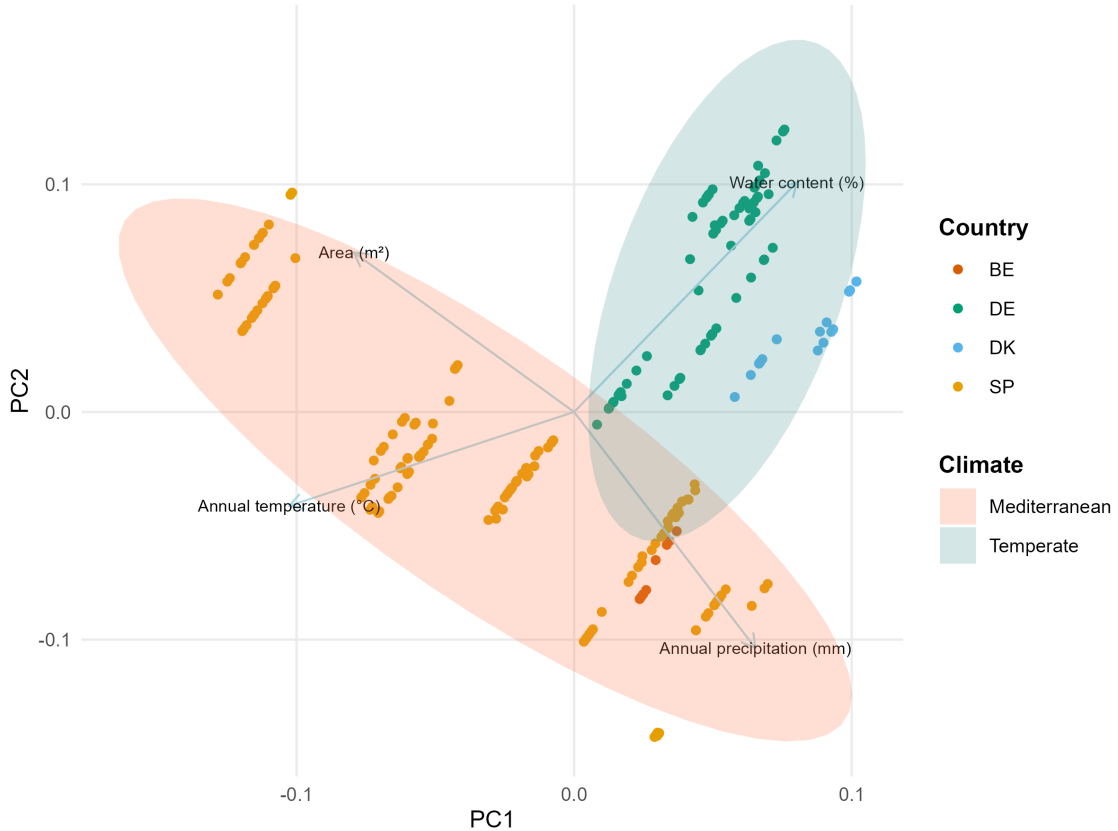


Figure S6. Principal Component Analysis (PCA) showing the distribution of ponds and the main environmental variables driving their separation. Points are coloured by country: Spain (yellow), Denmark (blue), Germany (green) and Belgium (orange), as indicated in the legend. Ellipses represent the confidence intervals for the climate groups: Mediterranean (orange) and Temperate (green). Each dot corresponds to an individual pond measurement.



WEOM and DOM PROTOCOL

First, we ground the sediment samples in a mixer mill (MM 400, Retsch) for 2 minutes at 400 Hz. We prepared a sediment-to-water solution at a 1:40 ratio (w/w) using ultrapure water (milli-Q) and placed it in an agitator (KS 260 basic, IKA®) set at 150 rpm inside a dark incubator at 4°C for 48h. Samples were then centrifuged for 10 minutes at 4500 rpm and 4°C (Avanti J-26 XPI, Beckman Coulter) and subsequently filtered through pre-combusted (450°C for 4 h) 0.7 µm GF/F filters (Whatman) followed by 0.2 nylon filters (Whatman®). The filtered water was used for analyses of dissolved organic matter (DOM) (see below) and dissolved organic carbon (DOC). For DOC measurements, samples were acidified to a pH of 2 by adding 1 M hydrochloric acid (HCl) and stored in darkness at 4 °C until analysis with a TOC-VCS total organic carbon analyzer (Shimadzu).

Dissolved Organic Matter (DOM)

We analysed DOM samples by their absorbance and fluorescence properties. We measured UV-VIS absorbance spectra (200-800 nm) using a Cary 4000 UV-Vis spectrophotometer (Agilent) with a 1 cm quartz cuvette. We processed the measurements using the Scan software. We used ultrapure water (Milli-Q) as the reference baseline before analyzing the samples and rinsed the cuvette thoroughly with ultrapure water between measurements to prevent cross-contamination. Before analysis, we equilibrated the samples to room temperature in the dark to avoid photochemical alterations. We calculated the absorption coefficient at wavelength λ (a_{λ} , m^{-1}) using the equation:

$$a_{\lambda} = a_{\lambda_0} e^{-S(\lambda_0 - \lambda)}$$

Where λ_0 is a reference wavelength, as described by (Stedmon et al., 2000).

We obtained the fluorescence Excitation Emission Matrix (EEMs) using a F-700 fluorescence spectrophotometer (Hitachi), with excitation wavelengths set between 250 and 450 nm in 3 nm intervals and emission wavelengths between 250 and 600 nm within 3 nm intervals. We processed the data using FL Solutions software. We measured an ultrapure water blank before sample analysis and subtracted it from each spectrum to correct for background fluorescence and eliminate solvent interference. We normalized fluorescence intensities using the Raman peak area of ultrapure water to ensure consistency across samples. We analysed the fluorescence and absorbance data of DOM using the R package StaRdom. (Pucher et al., 2019). Data pre-processing included smoothing to enhance peak detection, subtraction of blanks, correction for inner-filter effects and instrument-specific biases, removal of scattering regions (Rayleigh and Raman scattering) and normalization of fluorescence intensities using the Raman peak area.

We calculated classical fluorescence peaks B, T, A, M and C based on manual peak picking and indices as follows: the humification index (HIX; unitless) defined as the ratio between the peak area under the fluorescence emission spectra of 435–480 nm and 300–345 nm at an excitation wavelength of 254 nm; and the autochthonous productivity index or freshness index, biological index (BIX; unitless) calculated as the ratio of the fluorescence intensity emitted at 380 and 430 nm for an excitation of 310 nm. (Fellman et al., 2010; Gabor et al., 2014; Huguet et al., 2009). We also calculated the fluorescence index (FI; unitless) as the ratio of emission spectra of 475–500 nm at an excitation of 370 nm, and specific ultraviolet absorbance (SUVA; $\text{L mg}^{-1} \text{m}^{-1}$), an indicator of aromaticity, by dividing the UV coefficient absorbance at 254 nm by DOC (mg L^{-1}) (Weishaar et al., 2003). Additionally, we calculated absorbance at 254 nm and at 300nm, the ratio of absorbance at 250 to 365 nm (E2/E3), the ratio at 465 to 665 nm (E4/E6), the spectral slope for log-transformed absorption spectra ranges (S275-295, S350-400, S300-700) and the slope ratio (SR) of S275-295 to S350-400 (Helms et al., 2007).

Parallel Factor Analysis (PARAFAC)

We applied Parallel factor analysis (PARAFAC) following Murphy et al. (2013) to characterize the DOM and identify its main components. We used the StarRdom package (Pucher et al., 2019) to split the 252 EEMs via PARAFAC (Fig. S7). We processed data as previously outlined for DOM analysis, removed scatter peaks and normalized each to its total fluorescence.

We built several models to determine the most suitable number of components, using split-half analysis validation, core consistency, model fit, and residual examination. Based on these criteria, we selected a PARAFAC model with three components (Murphy et al., 2013). We identified the origin and nature of these components using the <https://openfluor.lablicate.com> platform, achieving 0.99 Tucker Congruence Coefficients (TCC) in both excitation and emission spectra, based on model matches in the repository (Table S3).

For the PARAFAC analysis, we evaluated the model stability and robustness through split-half analysis (splithalf function in staRdom package), which randomly split the dataset into subsets to ensure consistency across. We computed the Shift- and Shape-Sensitive Congruence (SSC) and the Total Congruence Coefficient (TCC), including the modified form (mTCC) that combines excitation and emission spectra (Parr et al., 2014; Wünsch et al., 2019). These metrics confirmed the stability and reproducibility of the final three-component model.

Additionally, we evaluated model adequacy using the core consistency diagnostic (eempf_corcondia function in package (Pucher et al., 2019)), which compared the modelled and actual data structure. Finally, we integrated the EEMqual parameter to synthesize model fit, core consistency, and split-half results (Bro and Vidal, 2011).

Figure S7. Excitation-Emission Spectra (EEM) of the dissolved organic matter components (C1, C2, C3) identified through PARAFAC analysis.

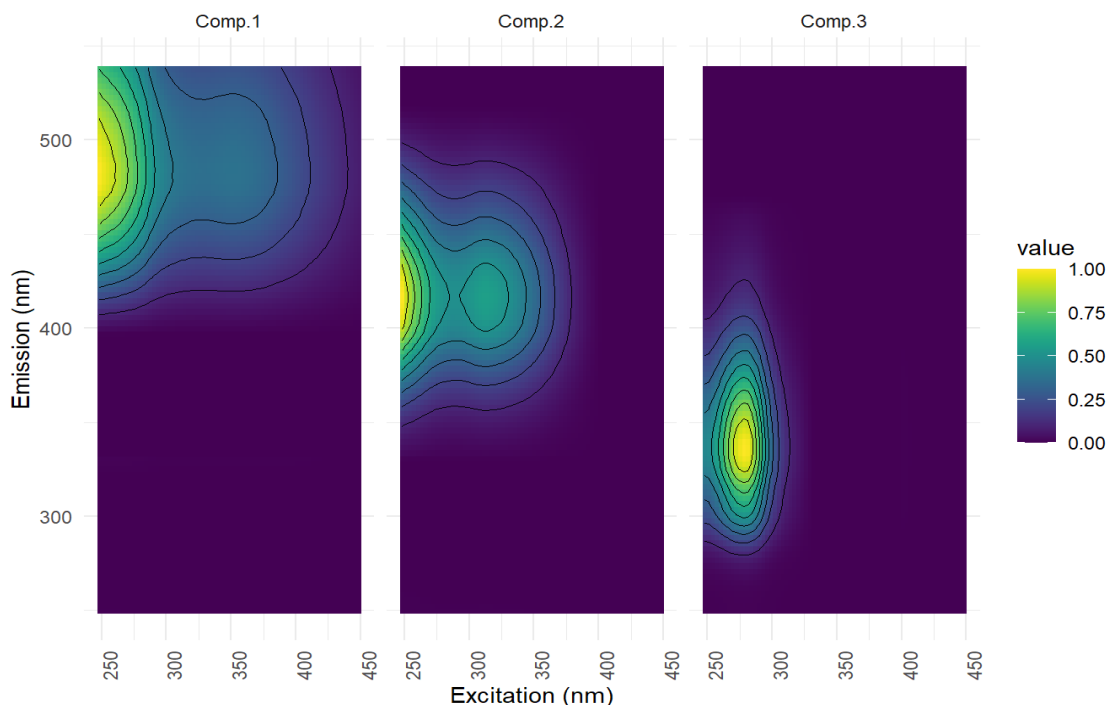


Table S3. Tucker congruence coefficients (TCC = 0.99) with published spectra from OpenFluor.org, including matching PARAFAC models and the corresponding components from related studies.

Components	N	Component and PARAFAC models matched	Description in papers
C1	18	Gueguen_NelsonR (C1); Shutova_G (C1); Combinations-R (C2); DarkOcean (C1); Peleato_biofilter (C2); Dainard_BeaufortBering2013 (C1); West_Greenland_Lakes (C1); Wheat (C2); Gueguen_JOIS (C1); Galveston_Bay (C1); Lake_Ice (C1); RecyclePC(C1); Combinations-O/R/S (C2); Forest soil with freeze-thaw disturbance (C2); Macaronesia_POS533 (C3); vale3C (C2); AmoRiver(C2); DOMIPEX (C1).	Terrestrial humic-like (plant/soil derived), traditionally peak C, Terrestrial origin, soil humic-like, terrestrial delivered OM, consisted of a combination of Peak A and Peak C, where terrestrial and non-processed OM would dominate, Fulvic-like.
C2	9	Sources_Soil_Leaf_leachate (C3); Gueguen_NelsonR (C2); poyang_five_river (C1); Shallow_Lakes_Patagonia(C1); Uryu (C1); Combinations-R (C1); ORCA_flume (C1); Lake_Ice(C2); Graeber_2012 (C1). NeusePOMDOM (C5); Microcystis_BB (C3); AntarcticIce (C3); LeafLeachate (C2); Graeber-Macro_Acces (C2); MRE Model (C6); Anammox_EPS (C1); Borisover_wastewater_treatment_plants (C1).	Humic-like, Humic-like fluorophores, probably composed of humic-like compounds derived from biological/microbial activity, traditionally peak A.
C3	8	Cite	Tryptophan-like, Autochthonous production, proteinaceous tryptophan-like matter, most ubiquitous, traditionally peak T
Models		Cite	DOI
DarkOcean		(Catalá et al., 2015)	https://doi.org/10.1038/ncomms6986
Graeber_2012		(Graeber et al., 2012)	https://doi.org/10.1016/j.scitotenv.2012.08.087
RecyclePC		(Murphy et al., 2011)	https://doi.org/10.1021/es103015e
NeusePOMDOM		(Osburn et al., 2012)	https://doi.org/10.1021/es3007723
Shallow-Lakes_Patagonia		(Soto Cárdenas et al., 2017)	https://doi.org/10.1002/eco.1872
Shutova_G		(Shutova et al., 2014)	https://doi.org/10.1016/j.watres.2014.01.053
AntarcticIce		(Stedmon et al., 2011)	https://doi.org/10.1029/2011JG001716
vale3C		(Amaral et al., 2016)	https://doi.org/10.1002/lno.10258
Wheat		(Romero et al., 2017)	https://doi.org/10.1016/j.geoderma.2017.06.029
LeafLeachate		(Wheeler et al., 2017)	https://doi.org/10.1002/2016JG003677
Microcystis_BB		(Bittar et al., 2015)	https://doi.org/10.1002/lno.10090
Peleato_biofilter		(Peleato et al., 2016)	https://doi.org/10.1016/j.chemosphere.2016.03.018
West_Greenland_Lakes		(Osburn et al., 2017)	https://doi.org/10.1002/2017JG003999
Sources_Soil_Leaf_leachate		(Garcia et al., 2018)	https://doi.org/10.1111/fwb.13114
poyang_five_river		(Yan et al., 2020)	https://doi.org/10.1007/s11356-020-09500-x
Borisover_wastewater_treatment_plants		(Cohen et al., 2014)	https://doi.org/10.1016/j.watres.2014.02.040
Galveston_Bay		(Gold-Bouchot et al., 2021)	https://doi.org/10.1007/s11356-021-14509-x
Anammox_EPS		(Jia et al., 2017)	https://doi.org/10.1021/acs.est.6b05761
ORCA_flume		(Weigelhofer et al., 2020)	https://doi.org/10.3390/w12113246
ArnoRiver		(Retelletti Brogi et al., 2020)	https://doi.org/10.1016/j.scitotenv.2020.139212
Forest_soil_with_freeze-thaw_disturbance		(Wu et al., 2021)	https://doi.org/10.1016/j.catena.2020.105058
Uryu		(Yamashita et al., 2021)	https://doi.org/10.1016/j.chemosphere.2021.12824
Gueguen_JOIS		(DeFrancesco and Guéguen, 2021)	https://doi.org/10.1029/2020JC016578
Gueguen_NelsonR		(Guéguen et al., 2016)	https://doi.org/10.1016/j.jmarsys.2016.05.005
Dainard_BeaufortBering2013		(Dainard and Guéguen, 2013)	https://doi.org/10.1016/j.marchem.2013.10.007
Lake_Ice		(Imbeau et al., 2021)	https://doi.org/10.1029/2020JG006233
Combinations-R		(Pitta and Zeri, 2021)	https://doi.org/10.1016/j.saa.2021.119800
Combinations-O/R/S		(Pitta and Zeri, 2021)	https://doi.org/10.1016/j.saa.2021.119800
Macaronesia_POS533		(Santana-Casiano et al., 2022)	https://doi.org/10.1021/acs.est.1c04512
DOMIPEX		(Catalán et al., 2018)	https://doi.org/10.1029/2018GB005919
Graeber-Macro_Access		(Graeber et al., 2021)	https://doi.org/10.1007/s10533-021-00809-4

Table S4. Fluorescence peaks of dissolved organic matter location and classification by Coble (1996).

Component label	Excitation location (nm)	Emission location (nm)	Traditional classification by Coble et.al (1996)	Description
C1	350	481	Peak C (Ex 330-350; Em 420-480)	Terrestrial, humic-like
C2	311	412	Peak A (Ex 250-260; Em 380-480)	Humic-like
C3	278	334	Peak T (Ex 270-280; Em 320-350)	Tryptophan-like

Table S5. Fluorescence components of dissolved organic matter: chemical interpretation and sources.

Component label	Chemical interpretation	Source
C1	Associated with low molecular weight humic-like substances. These are less aromatic and represent more degraded organic matter.	Often linked to microbially processed or autochthonous DOM, typically found in aquatic environments with significant microbial activity.
C2	Represents high molecular weight humic-like substances. These are highly aromatic compounds indicative of terrestrial inputs.	Derived from humification processes in soils and vegetation, reflecting terrestrial or allochthonous DOM inputs.
C3	Associated with protein-like substances, specifically aromatic amino acids such as tryptophan.	Indicates the presence of freshly produced, labile DOM. Often linked to microbial and phytoplankton activity, as well as wastewater inputs.

References

Amaral, V., Graeber, D., Calliari, D., and Alonso, C.: Strong linkages between DOM optical properties and main clades of aquatic bacteria, *Limnol Oceanogr*, 61, 906–918, <https://doi.org/10.1002/lno.10258>, 2016.

Bittar, T. B., Vieira, A. A. H., Stubbins, A., and Mopper, K.: Competition between photochemical and biological degradation of dissolved organic matter from the cyanobacteria *Microcystis aeruginosa*, *Limnol Oceanogr*, 60, 1172–1194, <https://doi.org/https://doi.org/10.1002/lno.10090>, 2015.

Bro, R. and Vidal, M.: EEMizer: Automated modeling of fluorescence EEM data, *Chemometrics and Intelligent Laboratory Systems*, 106, 68-92, <https://doi.org/https://doi.org/10.1016/j.chemolab.2010.06.005>, 2011.

Catalá, T. S., Reche, I., Fuentes-Lema, A., Romera-Castillo, C., Nieto-Cid, M., Ortega-Retuerta, E., Calvo, E., Álvarez, M., Marrasé, C., Stedmon, C. A., and Álvarez-Salgado, X. A.: Turnover time of fluorescent dissolved organic matter in the dark global ocean, *Nat Commun*, 6, 5986, <https://doi.org/10.1038/ncomms6986>, 2015.

Catalán, N., Casas-Ruiz, J. P., Arce, M. I., Abril, M., Bravo, A. G., del Campo, R., Estévez, E., Freixa, A., Giménez-Grau, P., González-Ferreras, A. M., Gómez-Gener, L., Lupon, A., Martínez, A., Palacin-Lizarbe, C., Poblador, S., Rasines-Ladero, R., Reyes, M., Rodríguez-Castillo, T., Rodríguez-Lozano, P., Sanpera-Calbet, I., Tornero, I., and Pastor, A.: Behind the Scenes: Mechanisms Regulating Climatic Patterns of Dissolved Organic Carbon Uptake in Headwater Streams, *Global Biogeochem Cycles*, 32, 1528–1541, <https://doi.org/10.1029/2018GB005919>, 2018.

Cohen, E., Levy, G. J., and Borisover, M.: Fluorescent components of organic matter in wastewater: Efficacy and selectivity of the water treatment, *Water Res*, 55, 323–334, <https://doi.org/10.1016/j.watres.2014.02.040>, 2014.

Dainard, P. G. and Guéguen, C.: Distribution of PARAFAC modeled CDOM components in the North Pacific Ocean, Bering, Chukchi and Beaufort Seas, *Mar Chem*, 157, 216–223, <https://doi.org/https://doi.org/10.1016/j.marchem.2013.10.007>, 2013.

DeFrancesco, C. and Guéguen, C.: Long-term Trends in Dissolved Organic Matter Composition and Its Relation to Sea Ice in the Canada Basin, Arctic Ocean (2007–2017), *J Geophys Res Oceans*, 126, e2020JC016578, <https://doi.org/https://doi.org/10.1029/2020JC016578>, 2021.

Fellman, J., Hood, E., and Spencer, R.: Fluorescence spectroscopy opens new windows into dissolved organic matter dynamics in freshwater ecosystems: A review, *Limnol Oceanogr*, 55, 2452–2462, <https://doi.org/10.4319/lo.2010.55.6.2452>, 2010.

Gabor, R., Baker, A., Mcknight, D., and Miller, M.: Fluorescence Indices and Their Interpretation, in: *Aquatic Organic Matter Fluorescence*, edited by: Coble, P. G., Lead, J., Baker, A., Reynolds, D. M., and Spencer, R. G. M., Cambridge University Press, Cambridge, 303–338, <https://doi.org/10.1017/CBO9781139045452.015>, 2014.

Garcia, R. D., Diéguez, M. del C., Gerea, M., Garcia, P. E., and Reissig, M.: Characterisation and reactivity continuum of dissolved organic matter in forested headwater catchments of Andean Patagonia, *Freshw Biol*, 63, 1049–1062, <https://doi.org/https://doi.org/10.1111/fwb.13114>, 2018.

Gold-Bouchot, G., Polis, S., Castañon, L. E., Flores, M. P., Alsante, A. N., and Thornton, D. C. O.: Chromophoric dissolved organic matter (CDOM) in a subtropical estuary (Galveston Bay, USA) and the impact of Hurricane Harvey, *Environmental Science and Pollution Research*, 28, 53045–53057, <https://doi.org/10.1007/s11356-021-14509-x>, 2021.

Graeber, D., Gelbrecht, J., Pusch, M. T., Anlanger, C., and von Schiller, D.: Agriculture has changed the amount and composition of dissolved organic matter in Central European headwater streams, *Science of The Total Environment*, 438, 435–446, <https://doi.org/https://doi.org/10.1016/j.scitotenv.2012.08.087>, 2012.

Graeber, D., Tenzin, Y., Stutter, M., Weigelhofer, G., Shatwell, T., von Tümpeling, W., Tittel, J., Wachholz, A., and Borchardt, D.: Bioavailable DOC: reactive nutrient ratios control heterotrophic nutrient assimilation—An experimental proof of the macronutrient-access hypothesis, *Biogeochemistry*, 155, 1–20, <https://doi.org/10.1007/s10533-021-00809-4>, 2021.

Guéguen, C., Mokhtar, M., Perroud, A., McCullough, G., and Papakyriakou, T.: Mixing and photoreactivity of dissolved organic matter in the Nelson/Hayes estuarine system (Hudson Bay, Canada), *Journal of Marine Systems*, 161, 42–48, <https://doi.org/https://doi.org/10.1016/j.jmarsys.2016.05.005>, 2016.

Helms, J., Stubbins, A., Ritchie, J., Minor, E., Kieber, D., and Mopper, K.: Absorption Spectral Slopes and Slope Ratios as Indicators of Molecular Weight, Source, and Photobleaching of Chromophoric Dissolved Organic Matter, *Limnol Oceanogr*, 53, 955–969, <https://doi.org/10.2307/40058211>, 2007.

Huguet, A., Vacher, L., Relexans, S., Saubusse, S., Froidefond, J. M., and Parlanti, E.: Properties of fluorescent dissolved organic matter in the Gironde Estuary, *Org Geochem*, 40, 706–719, <https://doi.org/https://doi.org/10.1016/j.orggeochem.2009.03.002>, 2009.

Imbeau, E., Vincent, W. F., Wauthy, M., Cusson, M., and Rautio, M.: Hidden Stores of Organic Matter in Northern Lake Ice: Selective Retention of Terrestrial Particles, Phytoplankton and Labile Carbon, *J Geophys Res Biogeosci*, 126, e2020JG006233, <https://doi.org/https://doi.org/10.1029/2020JG006233>, 2021.

Jia, F., Yang, Q., Liu, X., Li, X., Li, B., Zhang, L., and Peng, Y.: Stratification of Extracellular Polymeric Substances (EPS) for Aggregated Anammox Microorganisms, *Environ Sci Technol*, 51, 3260–3268, <https://doi.org/10.1021/acs.est.6b05761>, 2017.

Murphy, K. R., Hambly, A., Singh, S., Henderson, R. K., Baker, A., Stuetz, R., and Khan, S. J.: Organic Matter Fluorescence in Municipal Water Recycling Schemes: Toward a Unified PARAFAC Model, *Environ Sci Technol*, 45, 2909–2916, <https://doi.org/10.1021/es103015e>, 2011.

Murphy, K. R., Stedmon, C. A., Graeber, D., and Bro, R.: Fluorescence spectroscopy and multi-way techniques. PARAFAC, *Anal. Methods*, 5, 6557, <https://doi.org/10.1039/c3ay41160e>, 2013.

Osburn, C. L., Handsel, L. T., Mikan, M. P., Paerl, H. W., and Montgomery, M. T.: Fluorescence Tracking of Dissolved and Particulate Organic Matter Quality in a River-Dominated Estuary, *Environ Sci Technol*, 46, 8628–8636, <https://doi.org/10.1021/es3007723>, 2012.

Osburn, C. L., Anderson, N. J., Stedmon, C. A., Giles, M. E., Whiteford, E. J., McGinity, T. J., Dumbrell, A. J., and Underwood, G. J. C.: Shifts in the Source and Composition of Dissolved Organic Matter in Southwest Greenland Lakes Along a Regional Hydro-climatic Gradient, *J Geophys Res Biogeosci*, 122, 3431–3445, <https://doi.org/https://doi.org/10.1002/2017JG003999>, 2017.

Parr, T., Ohno, T., Cronan, C., and Simon, K.: comPARAFAC: a library and tools for rapid and quantitative comparison of dissolved organic matter components resolved by Parallel Factor Analysis, *Limnol Oceanogr Methods*, 12, 114–125, <https://doi.org/10.4319/lom.2014.12.114>, 2014.

Peleato, N. M., McKie, M., Taylor-Edmonds, L., Andrews, S. A., Legge, R. L., and Andrews, R. C.: Fluorescence spectroscopy for monitoring reduction of natural organic matter and halogenated furanone precursors by biofiltration, *Chemosphere*, 153, 155–161, <https://doi.org/https://doi.org/10.1016/j.chemosphere.2016.03.018>, 2016.

Pitta, E. and Zeri, C.: The impact of combining data sets of fluorescence excitation - emission matrices of dissolved organic matter from various aquatic sources on the information retrieved by PARAFAC modeling, *Spectrochim Acta A Mol Biomol Spectrosc*, 258, 119800, <https://doi.org/https://doi.org/10.1016/j.saa.2021.119800>, 2021.

Pucher, M., Wünsch, U., Weigelhofer, G., Murphy, K., Hein, T., and Graeber, D.: StaRdom: Versatile software for analyzing spectroscopic data of dissolved organic matter in R, *Water*, 11, <https://doi.org/10.3390/w11112366>, 2019.

Retelletti Brogi, S., Balestra, C., Casotti, R., Cossarini, G., Galletti, Y., Gonnelli, M., Vestri, S., and Santinelli, C.: Time resolved data unveils the complex DOM dynamics in a Mediterranean river, *Science of the Total Environment*, 733, 139212, <https://doi.org/10.1016/j.scitotenv.2020.139212>, 2020.

Romero, C. M., Engel, R. E., D'Andrilli, J., Chen, C., Zabinski, C., Miller, P. R., and Wallander, R.: Bulk optical characterization of dissolved organic matter from semiarid wheat-based cropping systems, *Geoderma*, 306, 40–49, <https://doi.org/https://doi.org/10.1016/j.geoderma.2017.06.029>, 2017.

Santana-Casiano, J. M., González-Santana, D., Devresse, Q., Hepach, H., Santana-González, C., Quack, B., Engel, A., and González-Dávila, M.: Exploring the Effects of Organic Matter Characteristics on Fe(II) Oxidation Kinetics in Coastal Seawater, *Environ Sci Technol*, 56, 2718–2728, <https://doi.org/10.1021/acs.est.1c04512>, 2022.

Shutova, Y., Baker, A., Bridgeman, J., and Henderson, R. K.: Spectroscopic characterisation of dissolved organic matter changes in drinking water treatment: From PARAFAC analysis to online monitoring wavelengths, *Water Res*, 54, 159–169, <https://doi.org/https://doi.org/10.1016/j.watres.2014.01.053>, 2014.

Soto Cárdenas, C., Gerea, M., García, P. E., Pérez, G. L., Diéguez, M. C., Rapacioli, R., Reissig, M., and Queimaliños, C.: Interplay between climate and hydrogeomorphic features and their effect on the seasonal variation of dissolved organic matter in shallow temperate lakes of the Southern Andes (Patagonia, Argentina): a field study based on optical properties, *Ecohydrology*, 10, e1872, <https://doi.org/https://doi.org/10.1002/eco.1872>, 2017.

Stedmon, C. A., Markager, S., and Kaas, H.: Optical Properties and Signatures of Chromophoric Dissolved Organic Matter (CDOM) in Danish Coastal Waters, *Estuar Coast Shelf Sci*, 51, 267–278, <https://doi.org/https://doi.org/10.1006/ecss.2000.0645>, 2000.

Stedmon, C. A., Thomas, D. N., Papadimitriou, S., Granskog, M. A., and Dieckmann, G. S.: Using fluorescence to characterize dissolved organic matter in Antarctic sea ice brines, *J Geophys Res Biogeosci*, 116, G03027, <https://doi.org/10.1029/2011JG001716>, 2011.

Weigelhofer, G., Jirón, T. S., Yeh, T.-C., Steniczka, G., and Pucher, M.: Dissolved Organic Matter Quality and Biofilm Composition Affect Microbial Organic Matter Uptake in Stream Flumes, *Water*, 12, 3246, <https://doi.org/10.3390/w12113246>, 2020.

Weishaar, J. L., Aiken, G. R., Bergamaschi, B. A., Fram, M. S., Fujii, R., and Mopper, K.: Evaluation of Specific Ultraviolet Absorbance as an Indicator of the Chemical Composition and Reactivity of Dissolved Organic Carbon, *Environ Sci Technol*, 37, 4702–4708, <https://doi.org/10.1021/es030360x>, 2003.

Wheeler, K. I., Levia, D. F., and Hudson, J. E.: Tracking senescence-induced patterns in leaf litter leachate using parallel factor analysis (PARAFAC) modeling and self-organizing maps, *J Geophys Res Biogeosci*, 122, 2233–2250, <https://doi.org/https://doi.org/10.1002/2016JG003677>, 2017.

Wu, H., Xu, X., Fu, P., Cheng, W., and Fu, C.: Responses of soil WEOM quantity and quality to freeze–thaw and litter manipulation with contrasting soil water content: A laboratory experiment, *Catena (Amst)*, 198, 105058, <https://doi.org/https://doi.org/10.1016/j.catena.2020.105058>, 2021.

Wünsch, U., Bro, R., Stedmon, C., Wenig, P., and Murphy, K.: Emerging patterns in the global distribution of dissolved organic matter fluorescence, *Analytical Methods*, 11, 888–893, <https://doi.org/10.1039/C8AY02422G>, 2019.

Yamashita, Y., Kojima, D., Yoshida, N., and Shibata, H.: Relationships between dissolved black carbon and dissolved organic matter in streams, *Chemosphere*, 271, 129824, <https://doi.org/https://doi.org/10.1016/j.chemosphere.2021.129824>, 2021.

Yan, C., Sheng, Y., Ju, M., Ding, C., Li, Q., Luo, Z., Ding, M., and Nie, M.: Relationship between the characterization of natural colloids and metal elements in surface waters, *Environmental Science and Pollution Research*, 27, 31872–31883, <https://doi.org/10.1007/s11356-020-09500-x>, 2020.